Acta Polytechnica CTU Proceedings **42**:55–60, 2023
https://doi.org/10.14311/APP.2023.42.0055

Published by the Czech Technical University in Prague

EXPERIMENTAL VALIDATION OF MOTION SENSOR PHYSILOG®5 APPLIED TO SHOULDER JOINT

Jan Krivošej*, Jana Garanová Krišťáková, Matej Daniel, Zbyněk Šika

Czech Technical University in Prague, Faculty of Mechanical Engineering, The Department of Mechanics, Biomechanics and Mechatronics, Technická 4, 160 00 Prague 6, Czech Republic

* corresponding author: jan.krivosej@fs.cvut.cz

Abstract. The main motivation of this paper is to verify the idea of using the Physilog®5 unit for the patients with shoulder movement difficulties. The attached sensor to the patient's arm then measures motion during which the patient should follow certain paths. Finally, if a patient has difficulty with motion requirements, some typical pattern for their problem should emerge. By analysing these patterns, a database of typical problems could be created, which could assist doctors in determining a patient's diagnosis.The experiment is focused on Physilog® concerning the 5^{th} generation. The goal is to experimentally identify and verify the performance of this generation during relatively large motions of the upper limb. For this purpose, an experimental stand representing spherical joint with an accurate absolute position sensing is assembled and calibrated. Subsequently, the three Physilog®5 sensors are mounted on this stand at different positions.

Keywords: Shoulder joint, motion sensor, wearable, experimental validation.

1. Introduction

Physilog®5 (P5) is well known and its applications are often related to lower limb motion sensing. In this case, the movement of the human lower limbs can be seen as planar. Another typical application assumption associated with the lower limb is the measurement of a relatively small angular range. These simplifications often lead to neglecting the acceleration in the perpendicular direction to the considered plane of movement of the limb and as a result the measuring unit often gives very good and relatively accurate outputs. However, during large movements of the shoulder joint this simplification cannot be made. Also, the absolute angular position drift that is present due to position acquisition through acceleration integration can be very significant. The article focused on drift reduction for highly dynamic movements is in [1]. Fasel et al. [2] also presents functional calibration and strap-down joint drift correction in alpine skiing for computing 3D joint angles. Palermo et al. [3] presents paper connected to the calibration of the lower limb sensing.

The paper connected to the lower limb motion sensing [4] shows validation of the P5 unit during walking when mounted in a shoe. Another validation of Physilog® sensor can be found in Lefeber at al. [5]. Special approach is shown in Su et al. [6] where wearable piezoelectric nanogenerators for self-powered body motion sensors are introduced.

The P5 unit is not the only option to sense the body/limb motion. Hamrs et al. [7] shows the Ethos unit, which is an alternative to the Physilog®5 and is described as: miniature orientation sensor for wearable human motion analysis. A different approach using a wearable functional arm movement sensing system is presented in Nguyen et al. [8], where the measurement is based on the concept of an optical linear encoder.

The aim of the paper is to experimentally verify the deployability, applicability and accuracy of the Physilog®5 motion measurement unit when used to measure absolute angular position, angular velocity and angular acceleration of the shoulder joint during large movements.

2. Experimental stand

The considered experimental stand consists of a spherical joint, which is assembled for this purpose as a rotational and an universal joint arranged in a serial configuration. Both the rotational and the universal joint are equipped with an accurate absolute position sensing. This approach is a very slight simplification of reality because the centre of the shoulder joint can move a little during motion. Further insight into this issue is provided, for example, in Wu wt al. [9].

The schematic view of the spherical joint is shown in Figure 1, which is hanging on the indicated frame connection. The angle measurement is provided by one Renishaw rotational absolute encoder RESM20USA150 with line count 16384 per revolution implemented for "Z" axis, two Renishaw rotational absolute encoders RESM20USA052 with line count 8192 per revolution implemented for "Y" and "X" axis and Renishaw's SiGNUM™ Si interface. The spherical motion is realized by simultaneous motion of "Z", "Y" and "X" axis (indicated in Figure 1). The "Z" axis motion is not restricted. Motion of "Y" and "X" axis

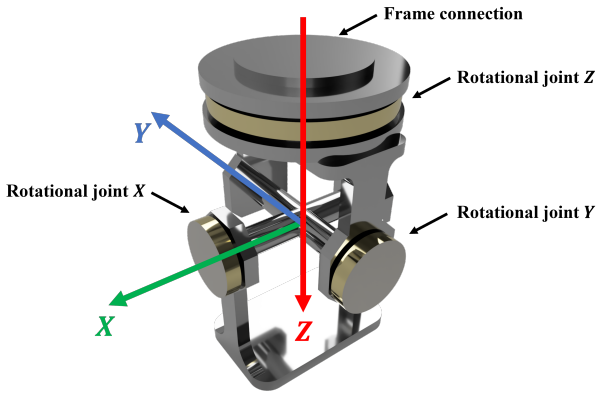

Figure 1. The schematic drawing of experimental stand of spherical joint with considered coordinate system.

are restricted to ±90 deg from the hanging position. A Physilog®5 unit is subsequently mounted on this assembly on the lower platform, which is together with the entire experimental stand setup shown in Figure 2.

3. Calibration of the experimental stand

Generally, calibration is a fundamental process of mechanism to ensure accuracy, reliability, and consistency in measurements.

The laser tracker (LT) Leica AT901 is used with the corner reflector (CR) for the calibration. The LT has accuracy 0.02 mm and the origin of the laser tracker measuring head is set approximately one meter from the CR in the rest position. The calibration setup is schematically shown in Figure 3, where the position of the corner reflector and the laser tracker with the reference point located at the origin of the laser tracker measuring head (the laser tracker is standing on the ground and the experimental stand is hanging on the indicated frame connection) are illustrated.

The used calibration procedure in the paper is based on modified Newton's method for overdetermined set of equations [10], [11]. The equations are given by constraints between dimensions of mechanism $\boldsymbol{d}$, measured variables $\boldsymbol{s}$ of three rotational joints and position of the reference point of external measuring $\boldsymbol{v}$. For the measurement in the j-th position one has

$$\boldsymbol{f}_j = \boldsymbol{f}(\boldsymbol{d}, \boldsymbol{s}_j, \boldsymbol{v}_j) = \boldsymbol{0}. \tag{1}$$

The real dimensions of mechanism $\boldsymbol{d}$ generally differ from the values $\widehat{\boldsymbol{d}}$ prescribed for manufacturing in design phase. However, one can consider them constant for all measurements. For n measurements one can rewrite Equation (1) into compact form

$$\boldsymbol{F}(\boldsymbol{d}, \boldsymbol{S}, \boldsymbol{V}) = \boldsymbol{0}, \tag{2}$$

Figure 2. The experimental stand with three P5 units mounted on the moving platform (connection to the frame can be seen at the top of Figure).

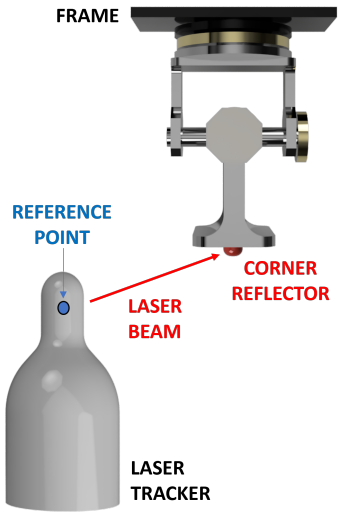

Figure 3. The schematic description of the calibration setup.

where $\boldsymbol{F} = [\boldsymbol{f}_1, \boldsymbol{f}_2, \ldots, \boldsymbol{f}_n]^T$, $\boldsymbol{S} = [\boldsymbol{s}_1, \boldsymbol{s}_2, \ldots, \boldsymbol{s}_n]^T$ and $\boldsymbol{V} = [\boldsymbol{v}_1, \boldsymbol{v}_2, \ldots, \boldsymbol{v}_n]^T$. Using Taylor series expansion yields

$$\boldsymbol{F}(\widehat{\boldsymbol{d}}, \boldsymbol{S}, \boldsymbol{V}) + \boldsymbol{J}_d \partial \boldsymbol{d} + \cdots = \boldsymbol{0}, \tag{3}$$

where $\boldsymbol{J}_d$ is the Jacobian matrix of partial derivatives of (2) with respect to $\boldsymbol{d}$. Considering the first term of Taylor series only from Equation (3) one can express $\boldsymbol{\partial d}$ using pseudoinversion of Jacobian matrix $\boldsymbol{J}_d$. Using iteration method the corrections can be found as

$$\boldsymbol{\partial d}_i = -(\boldsymbol{J}_{d_i}^T \boldsymbol{J}_{d_i})^{-1} \boldsymbol{J}_{d_i}^T + \boldsymbol{F}(\widehat{\boldsymbol{d}}_i, \boldsymbol{S}, \boldsymbol{V}), \tag{4}$$

and, subsequently, new values are iteratively obtained as

$$\boldsymbol{d}_{i+1} = \boldsymbol{d}_i + \boldsymbol{\partial d}_i. \tag{5}$$

Considering that the absolute Cartesian system is set by LT in the reference point, the whole kinematic model is described using transformation matrices as follows

$$\boldsymbol{r}_{0cr} = \boldsymbol{T}_{04} \boldsymbol{r}_{4cr}, \tag{6}$$

where $\boldsymbol{r}_{4cr} = [x_{4cr}, y_{4cr}, z_{4cr}, 1]^T$ is the radius vector of CR in the coordinate system of platform and $\boldsymbol{T}_{04}$ is given as

$$\boldsymbol{T}_{04} = \boldsymbol{T}_{01} \boldsymbol{T}_{12}(\varphi_{z\,M}) \boldsymbol{T}_{23}(\varphi_{y\,M}) \boldsymbol{T}_{34}(\varphi_{x\,M}), \tag{7}$$

where

$$\begin{aligned} \boldsymbol{T}_{01} = {} & \boldsymbol{T}_x(x_0) \boldsymbol{T}_y(y_0) \boldsymbol{T}_z(z_0) \boldsymbol{T}_{\varphi_x}(\varphi_{x0}) \\ & \boldsymbol{T}_{\varphi_y}(\varphi_{y0}) \boldsymbol{T}_{\varphi_z}(\varphi_{z0}), \end{aligned} \tag{8}$$

describing the position of the experimental demonstrator with respect to the position of the LT, angles $\varphi_{x\,M}$,$\varphi_{y\,M}$ and $\varphi_{z\,M}$ are measured by the encoders and

$$\begin{aligned} \boldsymbol{T}_{12}(\varphi_{z\,M}) = {} & \boldsymbol{T}_x(x_1) \boldsymbol{T}_y(y_1) \boldsymbol{T}_{\varphi_x}(\varphi_{x1}) \\ & \boldsymbol{T}_{\varphi_y}(\varphi_{y1}) \boldsymbol{T}_{\varphi_z}(\varphi_{z\,M}), \end{aligned}$$

$$\begin{aligned} \boldsymbol{T}_{23}(\varphi_{y\,M}) = {} & \boldsymbol{T}_x(x_2) \boldsymbol{T}_z(z_2) \boldsymbol{T}_{\varphi_x}(\varphi_{x2}) \\ & \boldsymbol{T}_{\varphi_z}(\varphi_{z2}) \boldsymbol{T}_{\varphi_y}(\varphi_{y\,M}), \end{aligned}$$

$$\begin{aligned} \boldsymbol{T}_{34}(\varphi_{x\,M}) = {} & \boldsymbol{T}_y(y_3) \boldsymbol{T}_z(z_3) \boldsymbol{T}_{\varphi_y}(\varphi_{y3}) \\ & \boldsymbol{T}_{\varphi_z}(\varphi_{z3}) \boldsymbol{T}_{\varphi_x}(\varphi_{x\,M}), \end{aligned} \tag{9}$$

describing the transformation from one system to the next one. The arising system has 21 unknown parameters to be calibrated. Namely, the vector of parameters to be calibrated is

$$\begin{aligned} \boldsymbol{d} = [& x_0, y_0, z_0, \varphi_{x0}, \varphi_{y0}, \varphi_{z0}, \\ & x_1, y_1, \varphi_{x1}, \varphi_{y1}, \\ & x_2, z_2, \varphi_{x2}, \varphi_{z2}, \\ & y_3, z_3, \varphi_{y3}, \varphi_{z3}, \\ & x_{4cr}, y_{4cr}, z_{4cr}]. \end{aligned} \tag{10}$$

The constraint equation in the form (1) is given as

$$\boldsymbol{r}_{0cr} - \boldsymbol{r}_{0cr_{LT}} = \boldsymbol{0}, \tag{11}$$

where $\boldsymbol{r}_{0cr_{LT}} = [x_{0cr_{LT}}, y_{0cr_{LT}}, z_{0cr_{LT}}, 1]^T$ is the radius-vector of the CR position measured by the LT.

The calibration process itself is divided into two phases. In the first phase, the data are measured. Specifically, the data are synchronously obtained from the LT and from the absolute encoders of the experimental stand. The motion of the stand is performed manually to reflect the motion of the upper limb. In the second phase, the obtained data are used for the offline calibration using iteration method described above ((11), (4) and (5)).

4. Experimental results

The experimental setup is shown in Figure 2, where three P5 units – Master (M), Slave 1 (S1) and Slave 2 (S2) – are mounted on the auxiliary platform (the simulation results are shown only for M and S1 for compactness, S2 gives very similar results in comparison with M and S1). The P5 units using bluetooth for the time synchonized during measurement. The motion of the platform is performed manually to simulate maximally similar conditions relative to the shoulder joint

The absolute measured angles are compared with the investigated sensor Physilog®5 using its own internal library from "Gait Up" (this library is locked and cannot be open or edited) and is used for offline data transformation after measurement, where raw data from accelerometer, gyroscope and magnetometer are transformed to quaternions and Euler angles in "Roll", "Pitch", "Yaw" (RPY) form. This computation is done offline after measurement. The important thing is the time sychnonisation of both measurements, which was done by taps on the platform with sensors before and after the measured motion. The synchronized time window is then framed by dashdotted vertical lines in related graphs.

The first experimental results shows the measurements considering the steady state (rest position). The comparison of the obtained data is shown in Figure 4. However, even for the steady state position, the M and S1 sensor data show a very significant drift of the "Z" axis. The remaining "X" and "Y" axis behaviour is on the other hand very good, but still slightly effected (S1) by the drifting "Z" axis. Note that the measurement range is from -180 to 180 deg and observed vertical line "jumps" represents exceeding of this limit, where measurement "jumps" from -180 to 180 deg and vice versa (this means, for example, that $\varphi_{z\,P}$ of sensor S1 in Figure 4 reaches approx. 2260 deg in 60 s).

A complementary view is subsequently shown in Figure 5, where the raw data from sensor M accelerometer and gyroscope during measured motion are plotted. The value a_z obtained from sensor M during the

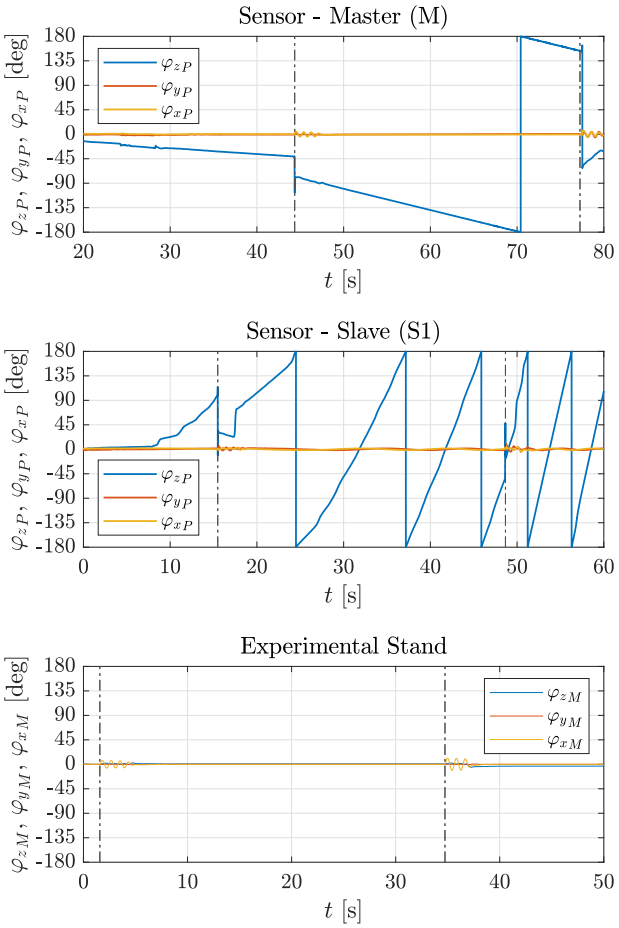

Figure 4. The obtained data from the sensor – Master (top), sensor – Slave 1 (middle) and experimental stand (bottom) during the steady state. The synchronized time window is framed by dashdotted vertical lines.

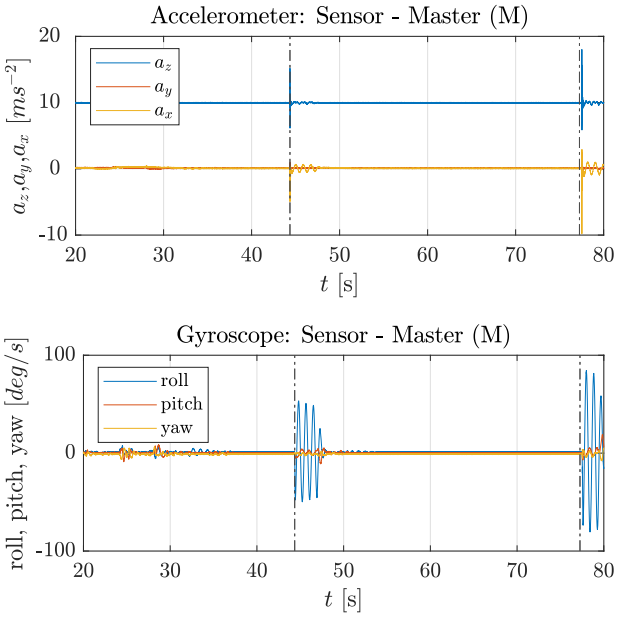

Figure 5. The raw data from accelerometer (top) and gyroscope (bottom) from the sensor – Master during the steady state. The synchronized time window is framed by dashdotted vertical lines.

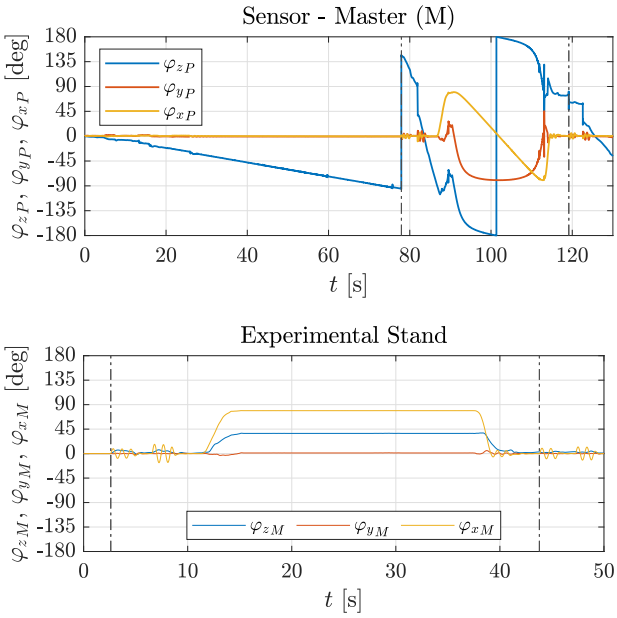

Figure 6. The obtained data from the sensor – Master (top) and experimental stand (bottom), where the considered steady state is obtained by deflection to another position. The synchronized time window is framed by dashdotted vertical lines.

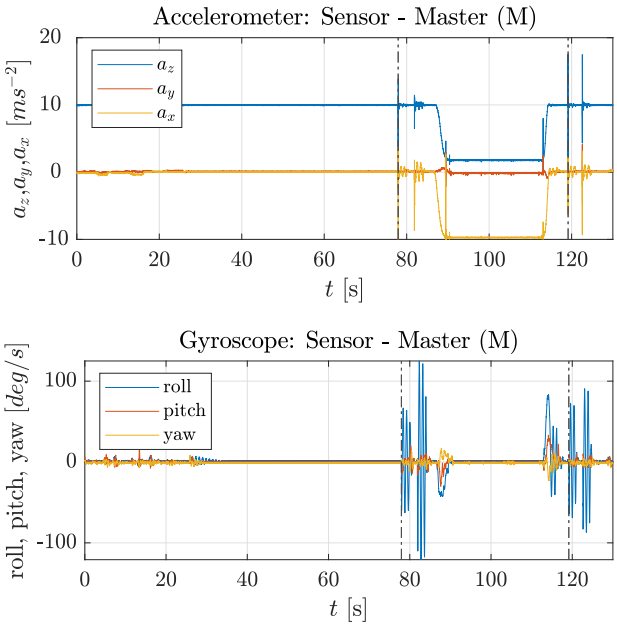

Figure 7. The raw data from accelerometer (top) and gyroscope (bottom) from the sensor – Master, where the considered steady state is obtained by deflection to another position. The synchronized time window is framed by dashdotted vertical lines.

steady state position measurement oscillates around 9.81 m s^{-2}, which represents the gravitational acceleration in "Z" axis direction. This acceleration should be removed from the accelerometer data during offline computation using internal library.

The second experimental results shows the measurements, where the considered steady state is obtained

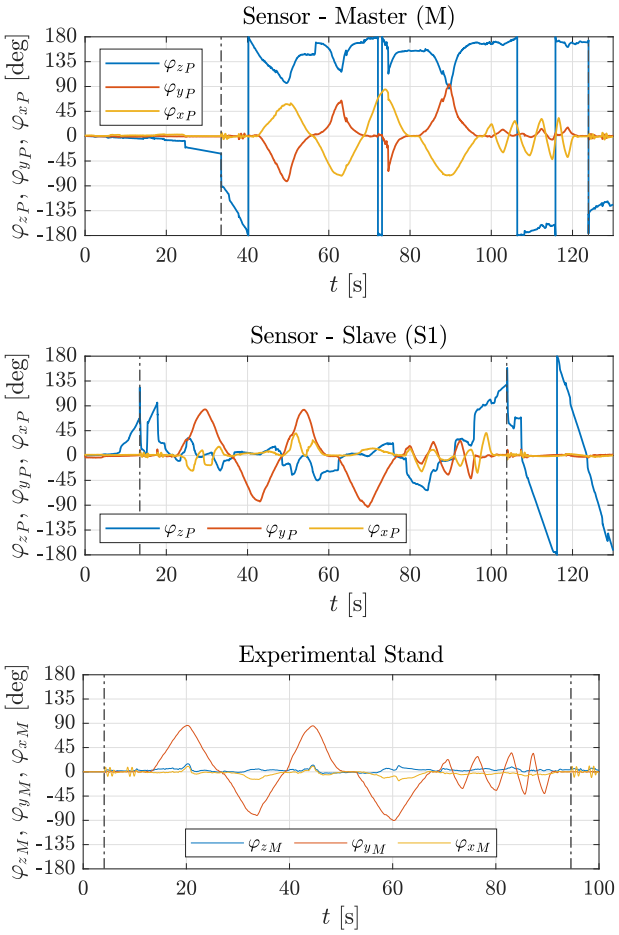

FIGURE 8. The obtained data from the sensor – Master (top), sensor – Slave 1 (middle) and experimental stand (bottom) during the pendulum motion around the "Y" axis. The synchronized time window is framed by dashdotted vertical lines.

by deflection to another position(different from the rest position). The comparison of the obtained data is shown in Figure 6. However, sensor M data shows a very significant drift of all three axis (plotted curves for the sensor S1 are very similar).

A complementary view is again shown in Figure 7, where the raw data from sensor M accelerometer and gyroscope during measured motion are plotted again. It can be seen that the gravitational acceleration vector effects mainly "Z" and "X" axes in this case. This acceleration should be again removed from the accelerometer data during offline computation using internal library.

The last presented experimental results shows the measurements, where the pendulum motion is performed manually around the "Y" axis. The comparison of the obtained data is shown in Figure 8. It can be seen that the swing motion pattern in comparison to the experimental stand is present at the sensor S1. However, sensor M suffers from "drift" more than sensor S1, which effect the measurement very badly.

5. Conclusion and future work

The experimental validation of sensor Physilog®5 has been proposed and studied. The experimental stand was designed to meet the kinematic requirement for spherical motion to simulate the kinematics of a shoulder joint. The design has been done as rotational and universal joint arranged in serial configuration. The angle measurement was provided by three Renishaw rotational absolute encoders and Renishaw's SiGNUM™ Si interface. The experimental stand has been calibrated using laser tracker Leica AT901. The movement of the platform with the sensor was performed manually to simulate maximally similar conditions relative to the shoulder joint.

The comparison of the experimental stand and Physilog®5 unit shows that the data directly obtained from the internal library during offline computation are not satisfactorily accurate. This fact is mainly seen in the axis, which is most of the time parallel or close to parallel to the vector of gravitational acceleration. This "drift" is very distinctive and has been present during each measurement. Its behaviour is very random and very strongly effects the the remaining two axes. It is shown that even the steady position suffers from the mentioned "drift".

Future work considers the use of raw data, additional filters, defining areas with minimum drift to obtain sufficiently appropriate data to obtain a reliable measurement for subsequent evaluation of the patient's shoulder movement difficulties.

Acknowledgements

This research was funded by the Czech Science Foundation project 23-06920S "Functionally biomimetic exoskeleton of human upper limb for selective muscle augmentation".

References

[1] B. Fasel, J. Sporri, J. Chardonnens, et al. Joint inertial sensor orientation drift reduction for highly dynamic movements. *IEEE Journal of Biomedical and Health Informatics* **22**(1):77–86, 2018. https://doi.org/10.1109/jbhi.2017.2659758

[2] B. Fasel, J. Spörri, P. Schütz, et al. Validation of functional calibration and strap-down joint drift correction for computing 3D joint angles of knee, hip, and trunk in alpine skiing. *PLOS ONE* **12**(7):e0181446, 2017. https://doi.org/10.1371/journal.pone.0181446

[3] E. Palermo, S. Rossi, F. Marini, et al. Experimental evaluation of accuracy and repeatability of a novel body-to-sensor calibration procedure for inertial sensor-based gait analysis. *Measurement* **52**:145–155, 2014. https://doi.org/10.1016/j.measurement.2014.03.004

[4] K. Carroll, R. Kennedy, V. Koutoulas, et al. Validation of shoe-worn Gait Up Physilog®5 wearable inertial sensors in adolescents. *Gait & Posture* **91**:19–25, 2022. https://doi.org/10.1016/j.gaitpost.2021.09.203

[5] N. Lefeber, M. Degelaen, C. Truyers, et al. Validity and reproducibility of inertial physilog sensors for spatiotemporal gait analysis in patients with stroke. *IEEE Transactions on Neural Systems and*

Rehabilitation Engineering **27**(9):1865–1874, 2019. https://doi.org/10.1109/tnsre.2019.2930751

[6] C. Su, X. Huang, L. Zhang, et al. Robust superhydrophobic wearable piezoelectric nanogenerators for self-powered body motion sensors. *Nano Energy* **107**:108095, 2023. https://doi.org/10.1016/j.nanoen.2022.108095

[7] H. Harms, O. Amft, R. Winkler, et al. ETHOS: Miniature orientation sensor for wearable human motion analysis. In *2010 IEEE Sensors*, pp. 1037–1042. IEEE, 2010. https://doi.org/10.1109/icsens.2010.5690738

[8] K. D. Nguyen, I.-M. Chen, Z. Luo, et al. A wearable sensing system for tracking and monitoring of functional arm movement. *IEEE/ASME Transactions on Mechatronics* **16**(2):213–220, 2011. https://doi.org/10.1109/tmech.2009.2039222

[9] G. Wu, F. C. van der Helm, H. D. Veeger, et al. ISB recommendation on definitions of joint coordinate systems of various joints for the reporting of human joint motion – Part II: shoulder, elbow, wrist and hand. *Journal of Biomechanics* **38**(5):981–992, 2005. https://doi.org/10.1016/j.jbiomech.2004.05.042

[10] P. Beneš, M. Valášek, Z. Šika, et al. Experiments with redundant parallel calibration and measuring machine RedCaM. *Applied and Computational Mechanics* **1**(2):387–392, 2007.

[11] P. Beneš, M. Valášek, J. Švéda. Measurement and calibration of machine tools in 6 DOFs in large workspace. *Journal of Machine Engineering* **9**(3):77–87, 2009.